Two-stage multipolar ordering in PrT_2Al$_{20}$ Kondo materials

Frederic Freyer,[1] Jan Attig,[1] SungBin Lee,[2] Arun Paramekanti,[3] Simon Trebst,[1] and Yong Baek Kim[3]

[1]*Institute for Theoretical Physics, University of Cologne, 50937 Cologne, Germany*
[2]*Department of Physics, Korea Advanced Institute of Science and Technology, Daejeon, 34141, Korea*
[3]*Department of Physics, University of Toronto, Toronto, Ontario, Canada M5S 1A7*

Among heavy fermion materials, there is a set of rare-earth intermetallics with non-Kramers Pr^{3+} $4f^2$ moments which exhibit a rich phase diagram with intertwined quadrupolar orders, superconductivity, and non-Fermi liquid behavior. However, more subtle broken symmetries such as multipolar orders in these Kondo materials remain poorly studied. Here, we argue that *multi-spin* interactions between local moments beyond the conventional two-spin exchange must play an important role in Kondo materials near the ordered to heavy Fermi liquid transition. We show that this drives a plethora of phases with coexisting multipolar orders and multiple thermal phase transitions, providing a natural framework for interpreting experiments on the Pr(T)$_2$Al$_{20}$ class of compounds.

I. INTRODUCTION

The celebrated Doniach picture of Kondo materials captures their evolution from magnetically ordered phases of local moments to the eventual heavy Fermi liquid phase when the local moments get fully incorporated into the Fermi sea [1–4]. Understanding the emergence of exotic ground states and quantum phase transitions in such heavy fermion systems is an important problem in condensed matter physics [5–9]. While magnetic ordering of a periodic array of local moments and its influence on Kondo physics has been studied extensively, subtle broken symmetries such as multipolar orders remain less explored [10–17]. In this context, recent experiments on the rare-earth intermetallics Pr(T)$_2$Al$_{20}$ (T = Ti,V) and PrIr$_2$Zn$_{20}$ are significant, showing rich phase diagrams as a function of temperature, pressure, and magnetic field, with quadrupolar orders, non-Fermi liquids, and superconductivity (SC) [18,18–32].

In these systems, Pr^{3+} ions have a non-Kramers ground state doublet, which acts as a pseudospin-1/2 degree of freedom on the diamond lattice [21,22]. As explained later, two components of this pseudospin carry a quadrupolar moment while the third component describes an octupolar moment, so their ordering would respectively correspond to time-reversal-even quadrupolar and time-reversal-odd octupolar symmetry breakings [33]. Such ordering is expected to be driven by a Kondo coupling to conduction electrons arising from T and Al in Pr(T)$_2$Al$_{20}$ (T = Ti, V). Indeed, experiments suggest ferroquadrupolar (F$\mathcal{Q}$) ordering in PrTi$_2$Al$_{20}$ at $T_1 \approx 2$ K, well above the superconducting transition temperature $T_c \approx 0.2$ K [18,19,21,27,32]. A recent series of experiments on PrV$_2$Al$_{20}$ discovered two closely spaced consecutive thermal transitions, at $T_1 \approx 0.8$ K and $T_2 \approx 0.7$ K, again well above the superconducting $T_c \approx 50$ mK, with evidence that the higher transition at T_1 is due to antiferroquadrupolar (AF$\mathcal{Q}$) order [18,30,34]. Understanding such multipolar orders is important

for clarifying the phase diagram of these heavy fermion systems, including the origin of SC.

The Doniach phase diagram of heavy fermion materials suggests that the weak Kondo coupling regime would lead to local-moment order driven by RKKY interactions, while the strong Kondo coupling regime would lead to a hybridized heavy Fermi liquid (FL) with a large Fermi surface (FS) [2–5,35]. The transition between these phases might be driven by increasing pressure or by choice of the T ion; for instance, PrV$_2$Al$_{20}$ appears to have stronger hybridization than PrTi$_2$Al$_{20}$ [18]. While attention has been mainly focused on the quadrupolar orders in such rare-earth intermetallics, our main observation is that the broader class of ordered phases could also involve the octupolar degrees of freedom driven by higher order *multispin* interactions, which have not been carefully explored.

One route to understanding the origin of such multispin interactions is to see that the 'small' to 'large' FS transition is driven by increasing hybridization. This will lead to the importance of higher order RKKY interactions, which can involve more than two spins. Alternatively, consider the Doniach phase diagram from the viewpoint of an orbital-selective Mott transition of the local moments [36,37]. In this case, the ordered phase with a small FS is an 'ordered Mott insulator' of the local moments, while the hybridized FL is a 'metallic phase' of the local moments. In analogy with organic Mott insulators, where four-spin ring exchange interactions near the Mott transition have been proposed to drive a quantum spin liquid with a spinon Fermi surface [38–42], we expect that upon approaching the 'Mott insulator' to 'metal' transition of the rare earth moments, similar multispin interactions will become significant and drive exotic phases of the local moments. This idea finds support in recent *ab initio* and phenomenological calculations on certain Kondo materials [43,44].

In this paper, we consider a frustrated local-moment model with two-spin and four-spin interactions, that are allowed by

symmetry associated with the local environment of Pr^{3+} ions and their coupling to the conduction electrons. Since our main interest is the interplay between different multipolar orders and their thermal phase transitions, we employ mean field theory and Monte Carlo simulations to investigate the thermal phase diagram of this model. Our key result is that such interactions can lead to ground states with *coexisting* multipolar orders; we show that this can lead to a single or two-stage multipolar thermal transition and present results on the effect of a magnetic field. We discuss how this provides a natural framework to interpret the experiments on $PrTi_2Al_{20}$ and PrV_2Al_{20}. Incorporating such multispin interactions may hold the key to understanding heavy fermion quantum criticality.

II. MODEL

In $Pr(T)_2Al_{20}$ (with $T =$ Ti, V), the $4f^2$ Pr^{3+} ion lives in a T_d local environment, arising from the Frank Kasper cage formed by 16 neighboring Al ions [22]. Inelastic neutron scattering and specific heat studies have shed light on the local spectrum of the Pr^{3+} ion, arising from crystal field splitting of the $J = 4$ angular momentum multiplet [18,21]. These indicate a Γ_3 non-Kramers doublet ground state separated from the next Γ_4 triplet of states by an energy gap $\sim$50 K. At temperatures $T \ll 50$ K, we can effectively ignore these excited crystal field multiplets [18]. Thus, for the low energy physics of these materials, especially the broken symmetry phases found at $T \lesssim 5$ K, it is sufficient to consider a model of conduction electrons Kondo coupled to this Γ_3 doublet, whose wave functions are [21,45]

$$\left|\Gamma_3^{(1)}\right\rangle = \frac{1}{2}\sqrt{\frac{7}{6}}\left|4\right\rangle - \frac{1}{2}\sqrt{\frac{5}{3}}\left|0\right\rangle + \frac{1}{2}\sqrt{\frac{7}{6}}\left|-4\right\rangle$$

$$\left|\Gamma_3^{(2)}\right\rangle = \frac{1}{\sqrt{2}}\left|2\right\rangle + \frac{1}{\sqrt{2}}\left|-2\right\rangle. \tag{1}$$

Using these, we can define the pseudospin-1/2 basis $\left|\uparrow\right\rangle \equiv \frac{1}{\sqrt{2}}(\left|\Gamma_3^{(1)}\right\rangle + i\left|\Gamma_3^{(2)}\right\rangle)$ and $\left|\downarrow\right\rangle \equiv \frac{1}{\sqrt{2}}(i\left|\Gamma_3^{(1)}\right\rangle + \left|\Gamma_3^{(2)}\right\rangle)$. We identify the corresponding pseudospin operators in terms of Stevens operators $O_{22} = \frac{\sqrt{3}}{2}(J_x^2 - J_y^2)$, $O_{20} = \frac{1}{2}(3J_z^2 - J^2)$, and $T_{xyz} = \frac{\sqrt{15}}{6}\overline{J_x J_y J_z}$ (overline denoting a symmetrized product), as $\tau_x = -\frac{1}{4}O_{22}$, $\tau_y = -\frac{1}{4}O_{20}$, and $\tau_z = \frac{1}{3\sqrt{5}}T_{xyz}$ [46,47]. Here, $(\tau_x, \tau_y) \equiv \vec{\tau}^\perp$ describes a time-reversal invariant quadrupolar moment, while τ_z describes a time-reversal odd octupolar moment. In addition, the point group symmetry of the Pr^{3+} ion includes an S_{4z} operation under which $\tau^\pm \to -\tau^\mp$, and a C_{31} operation under which $\tau^\pm \to e^{\pm i2\pi/3}\tau^\pm$.

With this in mind, we consider a symmetry-allowed model of short-distance two-spin exchange between the pseudospin-1/2 local moments $\vec{\tau}$, supplemented with the simplest four-spin interaction that couples quadrupolar and octupolar degrees of freedom,

$$H = \frac{1}{2}\sum_{i,j} J_{ij}\left(\vec{\tau}_i^\perp \cdot \vec{\tau}_j^\perp + \lambda\tau_i^z\tau_j^z\right)$$

$$- K\sum_{\langle\langle ij\rangle\langle km\rangle\rangle} \vec{\tau}_i^\perp \cdot \vec{\tau}_j^\perp \tau_k^z\tau_m^z. \tag{2}$$

We will assume $J_{ij} = J_1, J_2$ for nearest and next-nearest neighbors, respectively, and ignore further neighbor two-spin interactions. For the four-spin coupling, the notation $\langle\langle ij\rangle\langle km\rangle\rangle$ means that we consider a nearest-neighbor pair $\langle ij\rangle$ coupled to a distinct nearest-neighbor pair $\langle km\rangle$, such that the two pairs are separated by a single bond, leading to the shortest four-site cluster [48].

We consider the easy-plane regime, $\lambda < 1$, so that the two-spin interactions favor quadrupolar $\tau^{x,y}$ order over octupolar τ^z order as is observed in many of these compounds. While $J_1 < 0$ will drive F$\mathcal{Q}$ order, as observed in $PrTi_2Al_{20}$, increasing pressure might lead to AF$\mathcal{Q}$ orders, either via a frustrating $J_2/|J_1| > 0$ which leads to incommensurate spiral order (Sp$\mathcal{Q}$), or via a sign change $J_1 > 0$ which will lead to commensurate Néel quadrupolar order (N$\mathcal{Q}$) [18,21]. Our main insight is that while the two-spin interactions alone will favor pure quadrupolar order, four-spin interactions will generically lead to coexisting multipolar orders. For $K > 0$, quadrupolar orders with nearest-neighbor $\langle\vec{\tau}_i^\perp \cdot \vec{\tau}_j^\perp\rangle > 0$ will favor ferro-octupolar (F$\mathcal{O}$) order, while $\langle\vec{\tau}_i^\perp \cdot \vec{\tau}_j^\perp\rangle < 0$ will favor Néel octupolar (N$\mathcal{O}$) order; the F$\mathcal{O}$ and N$\mathcal{O}$ orders get switched when we consider $K < 0$.

Motivated by constructing the simplest model to capture the phenomenology of PrT_2Al_{20}, we will set $J_1 < 0$ for $PrTi_2Al_{20}$ which favors F$\mathcal{Q}$ order, and $J_1 > 0$ for PrV_2Al_{20} favoring N$\mathcal{Q}$ order. In both cases, we fix $J_2 > 0$ and $K > 0$, and study the phases and their properties as we vary $J_2/|J_1|$ and $K/|J_1|$. At the classical level of the analysis done here, we note that the model with $J_1 < 0$ maps onto the model with $J_1 > 0$ by changing $\vec{\tau} \to -\vec{\tau}$ on one sublattice; with this understanding, we will mainly focus on fixed $J_1 = +1$, but present results which are applicable for both systems.

III. GROUND STATE PHASE DIAGRAM

For $J_1 > 0$, consider an ansatz $\vec{\tau}_{A/B}^+ = \sqrt{1 - \eta^2}\exp(i\mathbf{q} \cdot \mathbf{r} \pm \frac{\phi}{2})$ for unit length spins on A/B sublattices, with $\tau_{A/B}^z = \pm\eta$. Here $\mathbf{q},\phi$ specify a spiral of $\vec{\tau}^\perp$ which is a generic Sp$\mathcal{Q}$ order with magnitude $\sqrt{1 - \eta^2}$. The limit $\mathbf{Q} = 0$ corresponds to the N$\mathcal{Q}$ state. This coexists with N$\mathcal{O}$ order of strength η. Let us define $F \equiv \cos\phi \cos\frac{q_x}{4}\cos\frac{q_y}{4}\cos\frac{q_z}{4} - \sin\phi \sin\frac{q_x}{4}\sin\frac{q_y}{4}\sin\frac{q_z}{4}$ and $G \equiv \cos\frac{q_x}{2}\cos\frac{q_y}{2} + \cos\frac{q_y}{2}\cos\frac{q_z}{2} + \cos\frac{q_z}{2}\cos\frac{q_x}{2}$, in terms of which we find the energy per site in the classical limit

$$\frac{E_{cl}}{N_{site}} = -2(J_1 - 18K\eta^2)(1 - \eta^2)F(\phi,\mathbf{q}) + 2J_1\lambda\eta^2$$

$$+ 6J_2\lambda\eta^2 + 2J_2(1 - \eta^2)G(\mathbf{q}). \tag{3}$$

Minimizing this variational energy with respect to $(\mathbf{q},\phi,\eta)$, we arrive at the $T = 0$ phase diagram, with phase boundaries depicted by solid lines in Fig. 1 for the choice $\lambda = 0$. Along the line $K = 0$, this phase diagram is identical with previous results obtained for Heisenberg spins on the diamond lattice, where $J_2/J_1 > 1/8$ drives a Néel to incommensurate spiral transition [49,50]. Our results show that $K \neq 0$ can induce
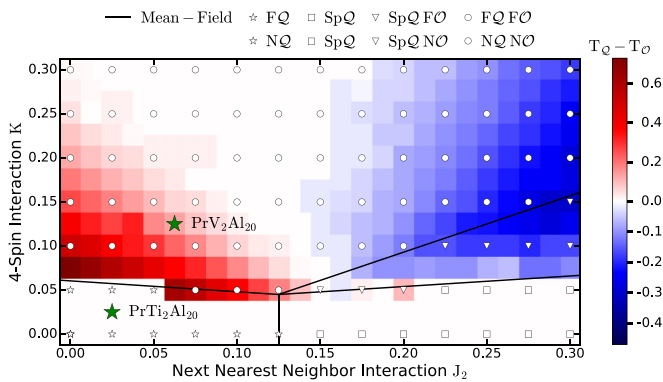
FIG. 1. Ground state phase diagram for the J_1-J_2-K model for fixed $J_1 = +1$, showing various ordered quadrupolar phases (N$\mathcal{Q}$ = Néel quadrupolar, Sp$\mathcal{Q}$ = spiral quadrupolar) as well as coexisting octupolar order (N$\mathcal{O}$ = Néel octupolar). For $J_1 = -1$, the phase diagram is identical but phases get relabelled as N$\mathcal{Q} \rightarrow$ F$\mathcal{Q}$ (ferroquadrupolar) and N$\mathcal{O} \rightarrow$ F$\mathcal{O}$ (ferrooctupolar). Solid lines are $T = 0$ mean field phase boundaries; points are obtained from Monte Carlo (MC) simulations on system sizes $L = 8$ (1024 spins) showing excellent agreement. Color indicates regions where we find two-stage thermal ordering in MC; the scale shows which broken symmetry (quadrupolar/octupolar) has a higher transition temperature. The "stars" indicate regions where we tentatively place the PrT_2Al$_{20}$ materials (with $J_1 < 0$ for PrTi$_2$Al$_{20}$ and $J_1 > 0$ for PrV$_2$Al$_{20}$).

N$\mathcal{Q}$/Sp$\mathcal{Q}$ phases which coexist with Ising N$\mathcal{O}$ order; we find qualitatively similar results for generic $\lambda < 1$ (see Appendix). For $J_1 < 0$, the N$\mathcal{Q}$/N$\mathcal{O}$ phases get replaced by F$\mathcal{Q}$/F$\mathcal{O}$ phases, while the spiral is modified by flipping $\vec{\tau}$ on one sublattice.

We have checked the $T = 0$ phase diagram in Fig. 1 using classical Monte Carlo (MC) simulations for system sizes up to $L = 8$ (with $2L^3 = 1024$ spins) down to $T/J_1 = 0.001$ at a large number of depicted points. The distinct ground states are best visualized in common origin plots of the spin vectors of configuration snapshots in the MC simulation as shown in Fig. 2. Depending on the τ^z order of the phase, characteristic $\vec{\tau}^\perp$ features (such as a ring for the spiral phase)
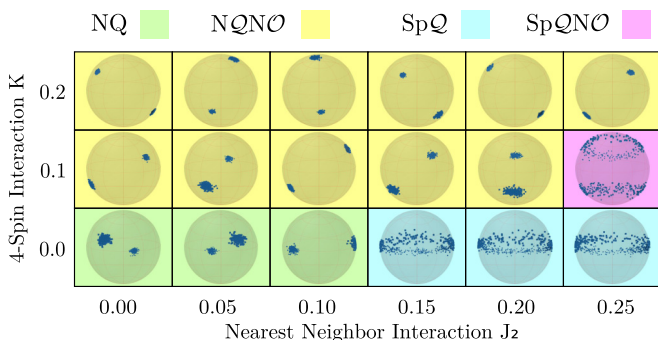

FIG. 2. Common-origin plots of the spin vectors in configuration snapshots from Monte Carlo simulations visualize the nature of the low-temperature ordering in the ground-state phase diagram of the J_1-J_2-K model in the J_2-K plane.
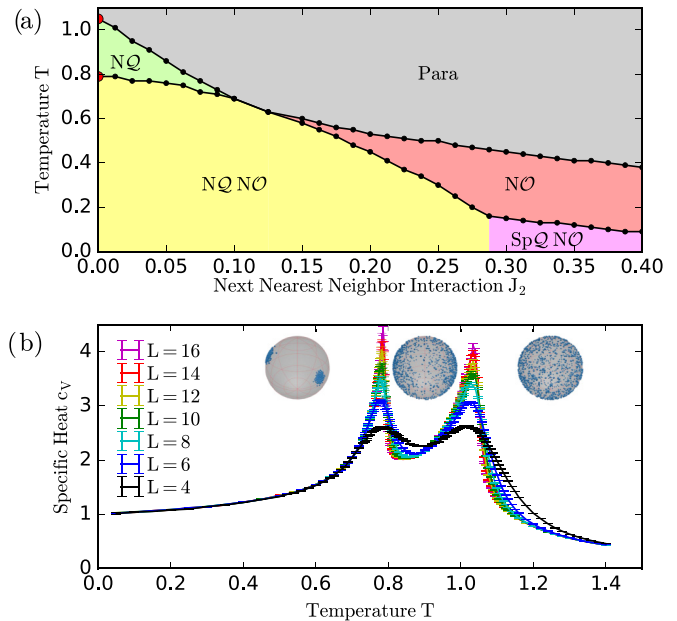

FIG. 3. (a) Finite-temperature phase diagram as a function of J_2 for fixed $J_1 = +1, K = 0.15$. The phase diagram is deduced from specific heat calculations which detects the phase transitions and from common origin plots which show the nature of the phases. (b) Illustrative plot of the specific heat versus temperature for $J_1 = +1$, $K = 0.15$, for fixed $J_2 = 0$ (in the N$\mathcal{Q}$N$\mathcal{O}$ phase) for various system sizes. Also shown are the common origin plots depicting the evolution from paramagnetic to N$\mathcal{Q}$ to N$\mathcal{Q}$N$\mathcal{O}$ order.

are shifted along the z axis in the common origin plot. The MC simulations clearly confirm our mean field ground state phase diagram.

IV. THERMAL TRANSITIONS

In order to explore the phase diagram of this model at nonzero temperatures, we have carried out extensive MC simulations for various system sizes and across a broad temperature regime. Figure 3(a) shows the phase diagram in the J_2-T plane at fixed $J_1 = 1, K = 0.15$. We find that both the N$\mathcal{Q}$N$\mathcal{O}$ and the Sp$\mathcal{Q}$N$\mathcal{O}$ phases generically undergo multiple phase transitions enroute to the high temperature paramagnet, with intervening phases which have pure octupolar or quadrupolar order. We deduce the existence of such transitions via peaks in the specific heat versus temperature, as illustrated in Fig. 3(b) for $J_2 = 0$, which get sharper with increasing system size. The nature of the phases can be deduced from common origin plots of snapshot MC configurations as shown for the N$\mathcal{Q}$N$\mathcal{O}$, N$\mathcal{Q}$, and paramagnetic phases in Fig. 3(b). Using extensive MC simulations of this sort over a wide range of parameters, we have compiled a detailed map of the two phase transitions, as shown in Fig. 1 with the color scale indicating regions where, upon lowering temperature, quadrupolar $\vec{\tau}^\perp$ orders first (red, $T_\mathcal{Q} - T_\mathcal{O} > 0$) or octupolar τ^z orders first (blue, $T_\mathcal{Q} - T_\mathcal{O} < 0$).
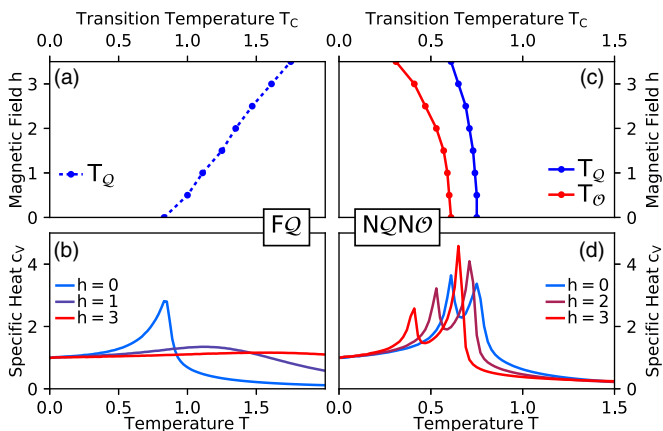
FIG. 4. Response of the F$\mathcal{Q}$ and N$\mathcal{Q}$N$\mathcal{O}$ phases to a [100] magnetic field. (a) Evolution of the transition temperature $T_\mathcal{Q}$ for the F$\mathcal{Q}$ state at zero field into a crossover line for nonzero field along [100] direction. The crossover temperature in (a) is obtained from specific heat scans as shown in (b), where the sharp peak signaling the transition at zero field becomes a rounded peak for nonzero h. (c) Evolution of transition temperatures $T_\mathcal{Q}$ and $T_\mathcal{O}$ for the N$\mathcal{Q}$N$\mathcal{O}$ state. In this case, the zero field transitions, signaled by the sharp specific heat peaks in (d), survive even for $h \neq 0$, with the field suppressing $T_\mathcal{O}$ more strongly than $T_\mathcal{Q}$.

V. MAGNETIC FIELD EFFECT

We next turn to the impact of an applied magnetic field as a further way to distinguish F$\mathcal{Q}$ from AF$\mathcal{Q}$ order. We begin by noting that the quadrupolar and octupolar moments of the Pr^{3+} Γ_3 doublet do not linearly couple to the magnetic field. The leading term is a quadratic-in-field coupling to the quadrupolar moment originating at second order perturbation theory in $\vec{h} \cdot \vec{J}$. This leads to nonzero matrix elements in the Γ_3 doublet with intermediate states arising from excited crystal field levels as $H_h = \sum_\alpha \frac{\vec{h} \cdot \vec{J} |\alpha\rangle \langle\alpha| \vec{h} \cdot \vec{J}}{\Delta(\alpha)} = \gamma h^2 (\frac{\sqrt{3}}{2}(\hat{h}_x^2 - \hat{h}_y^2)\tau_x + \frac{1}{2}(3\hat{h}_z^2 - 1)\tau_y)$ where $\alpha \in \Gamma_4, \Gamma_5$ refers to the two excited triplets above the ground state, $\Delta(\alpha)$ are the corresponding crystal field excitation energies, and $\gamma = (-\frac{14}{3\Delta(\Gamma_4)} + \frac{2}{\Delta(\Gamma_5)})$. The form of the coupling is simply understood on symmetry grounds; since the quadrupolar moments transform like an e_g doublet, the magnetic field couples to these moments with the same symmetries. Our model Eq. (2) has an XY symmetry, so that magnetic fields along the (100) direction or (110) direction act in an identical manner. However, the quadratic-in-field coupling to the quadrupole moment vanishes for a magnetic field along the (111) direction; instead, for this direction, the dominant term is a cubic-in-field coupling $\sim h^3(\hat{h}_x \hat{h}_y \hat{h}_z)\tau_z$ to the octupolar moment.

In order to illustrate the effect of the dominant coupling to the quadrupolar order, Fig. 4 shows the (100) magnetic field dependence for the F$\mathcal{Q}$ and N$\mathcal{Q}$N$\mathcal{O}$ phases which are presumed to be relevant to PrTi$_2$Al$_{20}$ and PrV$_2$Al$_{20}$, respectively. In the absence of an applied field, there is a direct continuous transition from the paramagnet into the F$\mathcal{Q}$ phase, but the (100) magnetic field converts this into a crossover, the crossover temperature increasing with the field as seen in Figs. 4(a) and 4(b). On the other hand, for the N$\mathcal{Q}$N$\mathcal{O}$ phase, both the phase

transitions (paramagnet to N$\mathcal{Q}$ and N$\mathcal{Q}$ to N$\mathcal{Q}$N$\mathcal{O}$) survive, and the transition temperatures decrease with increasing field. For this model, we find that the lower temperature transition (N$\mathcal{Q}$ to N$\mathcal{Q}$N$\mathcal{O}$) decreases more rapidly than the higher temperature transition. This can be understood based on Landau theory which will be discussed in Ref. [51] along with a detailed analysis for other field directions.

VI. COMPARISON TO EXPERIMENT

PrTi$_2$Al$_{20}$ exhibits a single phase transition from the paramagnetic phase into a broken symmetry F$\mathcal{Q}$ phase at $T_c \approx 2$ K, as identified from the fact that the sharp transition becomes a crossover in the presence of a magnetic field [21,22]. As seen in Fig. 1, the phase diagram with a ferromagnetic J_1 and a small $J_2, K > 0$ shows a (white) region with a single transition from the paramagnet into the F$\mathcal{Q}$ phase, which becomes a crossover in a nonzero (100) field as shown above. We thus place the parameters for the pseudospin-1/2 model for PrTi$_2$Al$_{20}$ in this region. Contrary to a single phase transition seen in PrTi$_2$Al$_{20}$, there exist two phase transitions in the case of PrV$_2$Al$_{20}$ [18,34]. In addition to $T_1 \approx 0.8$ K for the transition to N$\mathcal{Q}$ ordering, it has been observed that there is another phase transition slightly lower at $T_2 \approx 0.7$ K. It is possible that such two phase transitions originate from the ordering of quadrupolar moments (N$\mathcal{Q}$) and of octupolar moments (N$\mathcal{O}$), respectively. Again, our model with $J_1 > 0$ and with somewhat larger $J_2, K > 0$ does show a double transition, from paramagnet to N$\mathcal{Q}$, followed by a lower transition from N$\mathcal{Q}$ to N$\mathcal{Q}$N$\mathcal{O}$. There are extended parameter regimes seen in Fig. 1 with $J_1 > 0$ (light pink) where such closely spaced double transitions appear; thus we tentatively place PrV$_2$Al$_{20}$ in this regime of the phase diagram.

VII. DISCUSSION

In this paper, we have argued that multispin interactions should be generically important in Kondo materials near the ordered-to-hybridized FL transition. We have shown that this can lead to coexistence of quadrupolar and octupolar orders in the Pr(T)$_2$Al$_{20}$ systems. If we assume that PrV$_2$Al$_{20}$ has a stronger Kondo hybridization compared to PrTi$_2$Al$_{20}$, the two-stage thermal transitions seen in PrV$_2$Al$_{20}$ and a single transition in PrTi$_2$Al$_{20}$ would naturally be explained by relative importance of the multispin interactions in PrV$_2$Al$_{20}$ or the proximity to the ordered-to-hybridized FL transition. Further experiments and theory are needed to explore the dependence of the ordering temperatures on magnetic fields along various directions, which would further clarify the nature of the broken symmetries and the full phase diagram. Experiments to detect the octupolar order would also be invaluable. In this context, we note that μSR measurements to look for time-reversal breaking might be challenging since the electric field produced by the muon would break the non-Kramers degeneracy of the Γ_3 doublet for nearby Pr^{3+} ions. Nuclear magnetic resonance experiments might provide a complementary tool to detect the octupolar order. Finally, the presence of both quadrupolar and octupolar order may impact the non-Fermi liquid behavior near the putative ordered-to-hybridized FL quantum critical point. The pronounced non-Fermi liquid behavior seen above
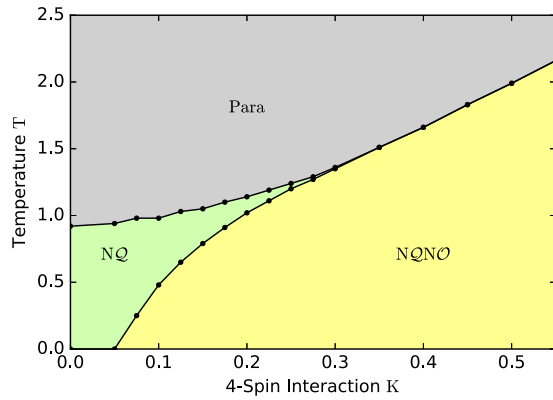
FIG. 5. Finite-temperature phase diagram for a constant $J_2 = 0$ cut through the phase diagram of Fig. 1 in the main paper.

FIG. 7. Double peak structure in specific heat scans for the two-stage ordering from paramagnet to N$\mathcal{O}$ to coexisting Sp$\mathcal{Q}$N$\mathcal{O}$ order at zero temperature ($J_2 = 0.25$; $K = -0.1$) for various system sizes.

the multipolar ordering temperature in PrV$_2$Al$_{20}$ may be the signatures of such a quantum critical point. Future work could explore the coupling between such unusual order parameters and conduction electrons, which can lead to quantum critical behavior.

APPENDIX: SUPPLEMENTAL NUMERICAL DATA

In this Appendix we present additional numerical data for the two-stage multipolar ordering transitions in various parts of the phase diagram of the J_1-J_2-K model presented in Fig. 1 in the main paper. Figures 5 and 6 exhibit finite-temperature phase diagrams for constant $J_2 = 0$ and $J_2 = 0.25$ cuts through the phase diagram of Fig. 1 in the main paper. In addition, Figs. 7 and 8 present explicit numerical data for specific heat scans revealing the two-stage thermal transitions into low-temperature sp$\mathcal{Q}$N$\mathcal{O}$ and N$\mathcal{Q}$N$\mathcal{O}$ orders, respectively.
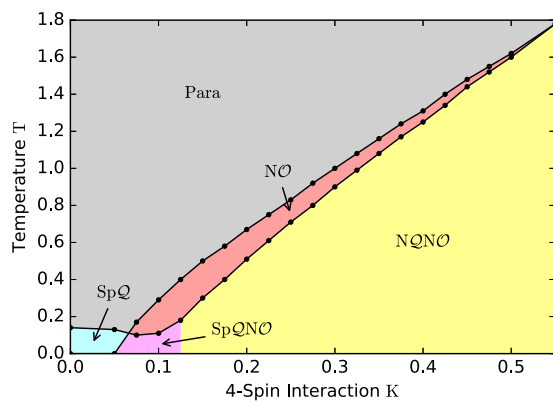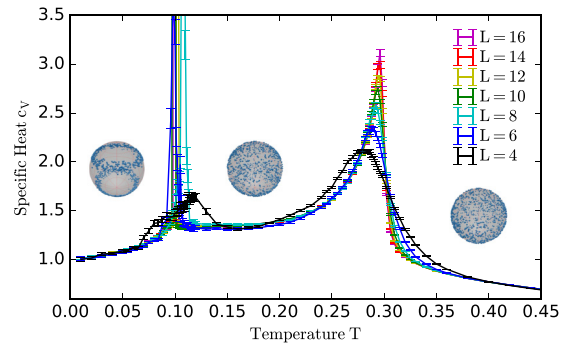

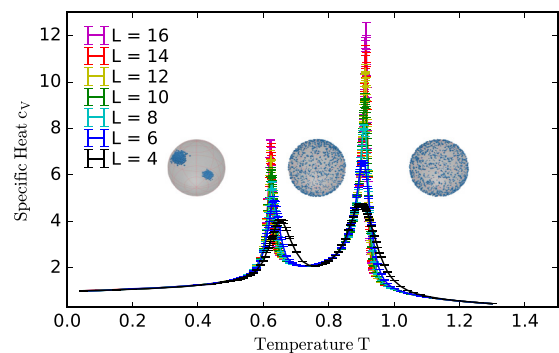FIG. 6. Finite-temperature phase diagram along a constant $J_2 = 0.25$ cut through the phase diagram of Fig. 1 in the main paper.

FIG. 8. Double peak structure in specific heat scans for the two-stage ordering from paramagnet to N$\mathcal{O}$ to the coexisting N$\mathcal{Q}$N$\mathcal{O}$ order at zero temperature ($J_2 = 0.35$; $K = -0.3$) for various system sizes.

[1] S. Doniach, The Kondo lattice and weak antiferromagnetism, Physica B+C **91**, 231 (1977).

[2] Melvin A. Ruderman and Charles Kittel, Indirect exchange coupling of nuclear magnetic moments by conduction electrons, Phys. Rev. **96**, 99 (1954).

[3] T. Kasuya, A theory of metallic ferro-and antiferromagnetism on Zener's model, Prog. Theor. Phys. **16**, 45 (1956).

[4] K. Yosida, Magnetic properties of Cu-Mn alloys, Phys. Rev. **106**, 893 (1957).

[5] S. G. R. Stewart, Heavy-fermion systems, Rev. Mod. Phys. **56**, 755 (1984).

[6] Z. Fisk, J. L. Sarrao, J. L. Smith, and J. D. Thompson, The physics and chemistry of heavy fermions, Proc. Natl. Acad. Sci. USA **92**, 6663 (1995).

[7] P. Coleman, C. Pépin, Q. Si, and R. Ramazashvili, How do fermi liquids get heavy and die? J. Phys.: Condens. Matter **13**, R723 (2001).

[8] P. Gegenwart, Q. Si, and F. Steglich, Quantum criticality in heavy-fermion metals, Nat. Phys. **4**, 186 (2008).

[9] Q. Si and F. Steglich, Heavy fermions and quantum phase transitions, Science **329**, 1161 (2010).

[10] P. Morin, D. Schmitt, and E. D. T. De Lacheisserie, Magnetic and quadrupolar properties of $PrPb_3$, J. Magn. Magn. Mater. **30**, 257 (1982).

[11] D. L. Cox, Quadrupolar Kondo Effect in Uranium Heavy-Electron Materials? Phys. Rev. Lett. **59**, 1240 (1987).

[12] D. L. Cox and A. Zawadowski, *Exotic Kondo Effects in Metals: Magnetic Ions in a Crystalline Electric Field and Tunelling Centres* (CRC Press, London, 1999).

[13] J. Kitagawa, N. Takeda, and M. Ishikawa, Possible quadrupolar ordering in a Kondo-lattice compound $Ce_3Pd_{20}Ge_6$, Phys. Rev. B **53**, 5101 (1996).

[14] R. Caciuffo, J. A. Paixão, C. Detlefs, M. J. Longfield, P. Santini, N. Bernhoeft, J. Rebizant, and G. H. Lander, Multipolar ordering in NpO_2 below 25 K, J. Phys.: Condens. Matter **15**, S2287 (2003).

[15] O. Suzuki, H. S. Suzuki, H. Kitazawa, G. Kido, T. Ueno, T. Yamaguchi, Y. Nemoto, and T. Goto, Quadrupolar Kondo effect in non-Kramers doublet system $PrInAg_2$, J. Phys. Soc. Jpn. **75**, 013704 (2005).

[16] Y. Kuramoto, H. Kusunose, and A. Kiss, Multipole orders and fluctuations in strongly correlated electron systems, J. Phys. Soc. Jpn. **78**, 072001 (2009).

[17] S. B. Lee, A. Paramekanti, and Y. B. Kim, Optical gyrotropy in quadrupolar Kondo systems, Phys. Rev. B **91**, 041104 (2015).

[18] A. Sakai and S. Nakatsuji, Kondo Effects and Multipolar Order in the Cubic $PrTr_2Al_{20}$ (Tr = Ti, V), J. Phys. Soc. Jpn. **80**, 063701 (2011).

[19] M. Koseki, Y. Nakanishi, K. Deto, G. Koseki, R. Kashiwazaki, F. Shichinomiya, M. Nakamura, M. Yoshizawa, A. Sakai, and S. Nakatsuji, Ultrasonic investigation on a cage structure compound $PrTi_2Al_{20}$, J. Phys. Soc. Jpn. **80**, SA049 (2011).

[20] A. Sakai and S. Nakatsuji, in *Journal of Physics: Conference Series*, Vol. 391 (IOP Publishing, Bristol, 2012), p. 012058.

[21] T. J. Sato, S. Ibuka, Y. Nambu, T. Yamazaki, T. Hong, A. Sakai, and S. Nakatsuji, Ferroquadrupolar ordering in $PrTi_2Al_{20}$, Phys. Rev. B **86**, 184419 (2012).

[22] T. Onimaru and H. Kusunose, Exotic Quadrupolar Phenomena in Non-Kramers Doublet Systems? The Cases of PrT_2Zn_{20} (T = Ir, Rh) and PrT_2Al_{20} (T = V, Ti)? J. Phys. Soc. Jpn. **85**, 082002 (2016).

[23] T. Onimaru, K. T. Matsumoto, Y. F. Inoue, K. Umeo, T. Sakakibara, Y. Karaki, M. Kubota, and T. Takabatake, Antiferroquadrupolar Ordering in a Pr-Based Superconductor $PrIr_2Zn_20$, Phys. Rev. Lett. **106**, 177001 (2011).

[24] Y. Shimura, Y. Ohta, T. Sakakibara, A. Sakai, and S. Nakatsuji, Evidence of a High-Field Phase in PrV2Al20 in a [100] Magnetic Field, J. Phys. Soc. Jpn. **82**, 043705 (2013).

[25] T. Onimaru, N. Nagasawa, K. T. Matsumoto, K. Wakiya, K. Umeo, S. Kittaka, T. Sakakibara, Y. Matsushita, and T. Takabatake, Simultaneous superconducting and antiferroquadrupolar transitions in $PrRh_2Zn_{20}$, Phys. Rev. B **86**, 184426 (2012).

[26] T. Onimaru, K. T. Matsumoto, Y. F. Inoue, K. Umeo, Y. Saiga, Y. Matsushita, R. Tamura, K. Nishimoto, I. Ishii, T. Suzuki *et al.*, Superconductivity and structural phase transitions in caged compounds RT_2Zn_{20} (R = La, Pr, T = Ru, Ir), J. Phys. Soc. Jpn. **79**, 033704 (2010).

[27] A. Sakai, K. Kuga, and S. Nakatsuji, Superconductivity in the ferroquadrupolar state in the quadrupolar Kondo lattice $PrTi_2Al_{20}$, J. Phys. Soc. Jpn. **81**, 083702 (2012).

[28] K. Matsubayashi, T. Tanaka, A. Sakai, S. Nakatsuji, Y. Kubo, and Y. Uwatoko, Pressure-Induced Heavy Fermion Superconductivity in the Nonmagnetic Quadrupolar System $PrTi_2Al_{20}$, Phys. Rev. Lett. **109**, 187004 (2012).

[29] K. Matsubayashi, T. Tanaka, J. Suzuki, A. Sakai, S. Nakatsuji, K. Kitagawa, Y. Kubo, and Y. Uwatoko, Heavy Fermion Superconductivity under Pressure in the Quadrupole System $PrTi_2Al_{20}$, in *Proceedings of the International Conference on Strongly Correlated Electron Systems (SCES2013)* (2014), p. 011077.

[30] M. Tsujimoto, Y. Matsumoto, T. Tomita, A. Sakai, and S. Nakatsuji, Heavy-Fermion Superconductivity in the Quadrupole Ordered State of PrV_2Al_{20}, Phys. Rev. Lett. **113**, 267001 (2014).

[31] K. Iwasa, K. T. Matsumoto, T. Onimaru, T. Takabatake, J.-M. Mignot, and A. Gukasov, Evidence for antiferromagnetic-type ordering of f-electron multipoles in $PrIr_2Zn_{20}$, Phys. Rev. B **95**, 155106 (2017).

[32] T. Taniguchi, M. Yoshida, H. Takeda, M. Takigawa, M. Tsujimoto, A. Sakai, Y. Matsumoto, and S. Nakatsuji, NMR Observation of Ferro-Quadrupole Order in $PrTi_2Al_{20}$, J. Phys. Soc. Jpn. **85**, 113703 (2016).

[33] R. Shiina, H. Shiba, and P. Thalmeier, Magnetic-field effects on quadrupolar ordering in a Γ 8-quartet system CeB_6, J. Phys. Soc. Jpn. **66**, 1741 (1997).

[34] M. Tsujimoto, Y. Matsumoto, and S. Nakatsuji, Anomalous specific heat behavior in the quadrupolar Kondo system PrV_2Al_{20}, in *Journal of Physics: Conference Series*, Vol. 592 (IOP Publishing, Bristol, 2015), p. 012023.

[35] H. v. Löhneysen, A. Rosch, M. Vojta, and P. Wölfle, Fermi-liquid instabilities at magnetic quantum phase transitions, Rev. Mod. Phys. **79**, 1015 (2007).

[36] L de' Medici, A. Georges, and S. Biermann, Orbital-selective Mott transition in multiband systems: Slave-spin representation and dynamical mean-field theory, Phys. Rev. B **72**, 205124 (2005).

[37] L. de' Medici, S. R. Hassan, M. Capone, and X. Dai, Orbital-Selective Mott Transition Out of Band Degeneracy Lifting, Phys. Rev. Lett. **102**, 126401 (2009).

[38] O. I. Motrunich, Variational study of triangular lattice spin-1/2 model with ring exchanges and spin liquid state in κ-(ET)$_2$Cu$_2$(CN)$_3$, Phys. Rev. B **72**, 045105 (2005).

[39] O. I. Motrunich and M. P. A. Fisher, d-wave correlated critical Bose liquids in two dimensions, Phys. Rev. B **75**, 235116 (2007).

[40] D. N. Sheng, O. I. Motrunich, S. Trebst, E. Gull, and M. P. A. Fisher, Strong-coupling phases of frustrated bosons on a two-leg ladder with ring exchange, Phys. Rev. B **78**, 054520 (2008).

[41] D. N. Sheng, O. I. Motrunich, and M. P. A. Fisher, Spin Bose-metal phase in a spin-1/2 model with ring exchange on a two-leg triangular strip, Phys. Rev. B **79**, 205112 (2009).

[42] T. Grover, N. Trivedi, T. Senthil, and P. A. Lee, Weak Mott insulators on the triangular lattice: possibility of a gapless nematic quantum spin liquid, Phys. Rev. B **81**, 245121 (2010).

[43] E. Mendive-Tapia and J. B. Staunton, Theory of Magnetic Ordering in the Heavy Rare Earths: Ab Initio Electronic Origin of Pair- and Four-Spin Interactions, Phys. Rev. Lett. **118**, 197202 (2017).

[44] Y. Akagi, M. Udagawa, and Y. Motome, Hidden Multiple-Spin Interactions As an Origin of Spin Scalar Chiral Order in Frustrated Kondo Lattice Models, Phys. Rev. Lett. **108**, 096401 (2012).

[45] K. Hattori and H. Tsunetsugu, Antiferro Quadrupole Orders in Non-Kramers Doublet Systems, J. Phys. Soc. Jpn. **83**, 034709 (2014).

[46] K. W. H. Stevens, Matrix elements and operator equivalents connected with the magnetic properties of rare earth ions, Proc. Phys. Soc. London, Sect. A **65**, 209 (1952).

[47] K. R. Lea, M. J. M. Leask, and W. P. Wolf, The raising of angular momentum degeneracy of f-electron terms by cubic crystal fields, J. Phys. Chem. Solids **23**, 1381 (1962).

[48] We note in passing that there are symmetry allowed three-spin interactions, but they are highly frustrated; these will be explored elsewhere.

[49] D. Bergman, J. Alicea, E. Gull, S. Trebst, and L. Balents, Order-by-disorder and spiral spin-liquid in frustrated diamond-lattice antiferromagnets, Nat. Phys. **3**, 487 (2007).

[50] S. B. Lee and L. Balents, Theory of the ordered phase in A-site antiferromagnetic spinels, Phys. Rev. B **78**, 144417 (2008).

[51] S. B. Lee, J. Attig, F. Freyer, A. Paramekanti, S. Trebst, and Y. B. Kim (unpublished).